Draft version October 7, 2019
Typeset using LaTeX **preprint2** style in AASTeX61

# DETECTION OF HE I 10830 Å ABSORPTION DURING THE TRANSIT OF A WARM NEPTUNE AROUND THE M-DWARF GJ 3470 WITH THE HABITABLE-ZONE PLANET FINDER

Joe P. Ninan,[1,2] Gudmundur Stefansson,[3,1,2] Suvrath Mahadevan,[1,2] Chad Bender,[4] Paul Robertson,[5] Lawrence Ramsey,[1,2] Ryan Terrien,[6] Jason Wright,[1,2,7] Scott A. Diddams,[8,9] Shubham Kanodia,[1,2] William Cochran,[10] Michael Endl,[10] Eric B. Ford,[1,2,11] Connor Fredrick,[8,9] Samuel Halverson,[12] Fred Hearty,[1,2] Jeff Jennings,[8,9] Kyle Kaplan,[4] Emily Lubar,[10] Andrew J. Metcalf,[13,8,9] Andrew Monson,[1,2] Colin Nitroy,[1,2] Arpita Roy,[14,15] and Christian Schwab[16]

[1] *Department of Astronomy & Astrophysics, 525 Davey Laboratory, The Pennsylvania State University, University Park, PA, 16802, USA*
[2] *Center for Exoplanets and Habitable Worlds, 525 Davey Laboratory, The Pennsylvania State University,University Park, PA, 16802, USA*
[3] *NASA Earth and Space Science Fellow*
[4] *Steward Observatory, University of Arizona, Tucson, Arizona 85721, USA*
[5] *Department of Physics and Astronomy, University of California-Irvine, Irvine, California 92697, USA*
[6] *Department of Physics and Astronomy, Carleton College, Northfield, Minnesota 55057, USA*
[7] *Penn State Astrobiology Research Center, University Park, PA 16802, USA*
[8] *National Institute of Standards and Technology, 325 Broadway, Boulder CO, 80305 USA*
[9] *Department of Physics, University of Colorado, 2000 Colorado Ave, Boulder CO, 80309. USA*
[10] *Department of Astronomy and McDonald Observatory, University of Texas at Austin, 2515 Speedway, Stop C1400, Austin, TX 78712, USA*
[11] *Institute for CyberScience, The Pennsylvania State University, 525 Davey Laboratory, University Park, PA 16802, USA*
[12] *Jet Propulsion Laboratory, California Institute of Technology, 4800 Oak Grove Drive, Pasadena, CA 91109*
[13] *Space vehicles Directorate, Air Force Research Laboratory, 3550 Aberdeen Ave SE, Kirtland AFB, NM 87117 USA*
[14] *Millikan Prize Postdoctoral Fellow*
[15] *California Institute of Technology, 1200 E California Blvd, Pasadena, California 91125, USA*
[16] *Department of Physics and Astronomy, Macquarie University, Balaclava Road, North Ryde, NSW 2109, Australia*

(Received; Revised; Accepted)

Submitted to AAS Journals



## ABSTRACT

Understanding the dynamics and kinematics of out-flowing atmospheres of hot and warm exoplanets is crucial to understanding the origins and evolutionary history of the exoplanets near the evaporation desert. Recently, ground based measurements of the meta-stable Helium atom's resonant absorption at 10830 Å has become a powerful probe of the base environment which is driving the outflow of exoplanet atmospheres. We report the detection of He I 10830 Å in absorption (equivalent width $\sim$

Corresponding author: Joe P. Ninan
jpn23@psu.edu

$0.012 \pm 0.002$ Å) in the exosphere of a warm Neptune orbiting the M-dwarf, GJ 3470, during three transits using the Habitable Zone Planet Finder (HPF) near infrared spectrograph. This marks the first reported detection of He I 10830 Å atmospheric absorption for a planet orbiting a M-dwarf. Our detected absorption is broad and its blueshifted wing extends to -36 km/sec, the largest reported in the literature to date. We modelled the state of Helium atoms in the exosphere of GJ3470b based on assumptions on the UV and X-ray flux of GJ 3470, and found our measurement of flux-weighted column density of meta-stable state He $= 2.4 \times 10^{10} \mathrm{cm}^{-2}$, derived from our transit observations, to be consistent with model, within its uncertainties. The methodology developed here will be useful to study and constrain the atmosphere outflow models of other exo-planets, like GJ 3470b, which are near the edge of the evaporation desert.

## 1. INTRODUCTION

The conventional probe for escaping atmospheres has been the Ly$\alpha$ absorption from the ionized exosphere during a planetary transit. This technique has produced exosphere discoveries around hot Jupiters, and hot and warm Neptunes, e.g., HD 209458b (Vidal-Madjar et al. 2003), GJ 436b (Kulow et al. 2014), and GJ 3470b (Bourrier et al. 2018). Ehrenreich et al. (2015) mapped an extended comet-like trail of escaping atmosphere from GJ 436b using the absorption signatures in the blue wings of Ly$\alpha$. Bourrier et al. (2018) performed a similar analysis for GJ 3470b using Ly$\alpha$ observations from HST and detected an extended exosphere with neutral hydrogen around GJ 3470b.

While Ly$\alpha$ is a powerful probe of evaporating atmospheres, it has two major drawbacks. The extinction loss due to interstellar absorption of Ly$\alpha$, as well as the contamination from geocoronal emission, render the central core of the Ly$\alpha$ line unusable. This implies one can probe only the high velocity regions of the exo-spheres via fitting the wings of the Ly$\alpha$ line. The UV observations also have to be done from space—above the Earth's atmosphere—rendering them expensive and hard to do for a large number of systems.

Oklopčić & Hirata (2018) recently suggested the absorption lines of a metastable state of Helium at 10830 Å as an alternative probe of evaporating exoplanet atmospheres. He I 10830 Å lines are not affected by the interstellar medium, and are observable from the ground using high resolution near-infrared spectrographs. Since the core of the line is accessible, even the low velocity base regions of the outflowing exosphere is detectable. High resolution spectra enable us to isolate the stellar spectrum from the planet's absorption spectrum which is modulated by the radial velocity of the planet. High resolution is also crucial for removing contamination from narrow telluric absorption lines for ground based observations.

The search for He I 10830 Å absorption is not new. Seager & Sasselov (2000) proposed that this would be a large signature in F9V type star, HD 209458, though a search by Moutou et al. (2003) with VLT/ISAAC did not yield a detection. Recently, a handful of detections were made successfully around K-star planets, namely WASP-107b (Spake et al. 2018; Allart et al. 2019), HD 189733 b (Salz et al. 2018), HAT-P-11b (Mansfield et al. 2018; Allart et al. 2018) and WASP-69b (Nortmann et al. 2018).

In this paper, we report the detection of He I 10830 Å during the transit of GJ 3470b, a warm Neptune orbiting an M-dwarf star, using the Habitable-zone Planet Finder (HPF) on the 10 m Hobby-Eberly Telescope (HET) at McDonald Observatory. Section 2 outlines our HPF observations. We discuss our He I 10830 Å detection and associated modelling in Section 3, and we finally summarize our key conclusions in Section 4.

## 2. OBSERVATIONS AND DATA REDUCTION

We observed GJ 3470 at different phases of GJ 3470b's orbit using the Habitable-zone Planet Finder (HPF) spectrograph (Mahadevan et al. 2014; Metcalf et al. 2019). HPF is a near-infrared precision radial velocity spectrograph covering the wavelength regime of 8079 – 12786 Å at a resolution of R$\sim$55,000. Due to the HET design (Ramsey et al. 1998; Shetrone et al. 2007), we are limited to observe for a track length of $\sim$1 hr per night at GJ 3470's declination. We observed three transits of GJ 3470b on 2018-11-30 UT, 2019-01-19 UT, and 2019-04-16 UT, when the transits aligned with the observable window of HET. Out-of-transit observations were conducted on 2019-01-04 UT, 2019-01-27 UT and 2019-04-17 UT. Three frames of 916 seconds integration time were taken in each of the $\sim$1 hr tracks during in-transit and out-transit observations. The median signal-to-noise ratio of individual spectra was ∼140 per pixel.

Echelle spectra of GJ 3470 from HPF were reduced using our HPF spectral extraction pipeline. The pipeline first generates 2D flux images (in units of electrons per second) from the up-the-ramp H2RG readout data (Ninan et al. 2018). A formal pixel-by-pixel variance image is also generated and propagated through the pipeline. The simultaneous Star, Sky and Calibration fiber spectra (as well as variance estimates) are then extracted from this 2D image (Kaplan et al. 2018).

To minimise scattered light contamination, no simultaneous calibration light spectra was used during the observations. The wavelength calibration of the extracted spectra was done using a custom built frequency stabilised laser comb (LFC; Metcalf et al. 2019) measurements taken throughout the night, inversely weighted by the time difference between science and LFC images following the methodology in Metcalf et al. (2019) and Stefansson et al. 2019 (in prep). All of our analysis and plots are in vacuum wavelengths. The spectra are then flat corrected and deblazed.

Sky emission lines are subtracted using the simultaneous sky spectrum. This step also subtracts out the smooth background scattered light due to the proximity of the sky fiber to the star fiber image on the detector. A 7 pixel median filter smoothing was applied to the sky fiber data in regions devoid of emission lines to reduce the noise in continuum regions of sky emission spectrum. Stellar continuum was also removed by fitting a quadratic polynomial continuum. Telluric absorption lines were corrected using an improved version of TERRASPEC code (Bender et al. 2012), a wrapper around `LBLRTM` (Clough et al. 2005). A good sky emission line subtraction and telluric absorption correction was crucial since He I 10830 Å falls close to a strong OH emission lines as well as water absorption lines. The residuals in the sky and telluric corrected regions are still dominated by imperfect modelling and they are significantly above the photon noise.

Due to HET's constrained pointing—resulting in short (∼1 hour long) observation windows on GJ 3470—our out-of-transit and in-transit observations are spread across multiple nights. To down-weight the region of the spectrum partially recovered from sky and telluric corrections, the variances of those regions are artificially inflated by a large factor (∼100). In doing so, this allows us to combine multiple epochs (with different barycentric shifts) weighted by the variance and obtain an average spectrum without residual artifacts from imperfect telluric and sky emission subtraction dominating.

The GJ 3470 system's parameters used in this paper are summarized in Table 1.

## 3. RESULTS AND DISCUSSION

### 3.1. *Detection of He I 10830 Å During Transit*

The blue curve at the top of Figure 1 shows the weighted average of all the in-transit spectra from three transit epochs divided by the average of the out-of-transit spectra. The vacuum wavelengths of the He 10830 Å triplet in the planet's rest frame are marked by the orange vertical lines. Since the telluric correction as well as the sky emission line subtraction are not perfect, regions of sky/telluric contamination have enlarged error bars as discussed in Section 2. The weighted average of all combinations of transits taken two at a time is also shown in the curves below. The peak observed 10833 Å is not present in Transit 2 and 3, it is only seen in Transit 1. However, since 10833 Å was separated from the telluric band only during Transit 1, it did not get averaged out in the final weighted average. Hence, we are cautiously inclined to believe that this peak inside the broad absorption is real. As a null result comparison,

**Table 1.** Orbital parameters of GJ 3470b used in calculation

| Parameter | Value | Description | Reference |
|---|---|---|---|
| $\gamma$ | 26.090 | Absolute stellar RV ( $\mathrm{km\,s^{-1}}$) | Gaia Collaboration et al. (2018) |
| $T_{\rm eff}$ | 3600 | Stellar effective temperature (K) | Awiphan et al. (2016) |
| [Fe/H] | 0.20 | Stellar metallicity | Awiphan et al. (2016) |
| $\log g$ | 4.695 | Stellar surface gravity | Awiphan et al. (2016) |
| $M_*$ | 0.51 ±0.06 | Stellar mass ($M_\odot$) | Biddle et al. (2014) |
| $R_*$ | 0.48 ±0.04 | Stellar radius ($R_\odot$) | Biddle et al. (2014) |
| $T_0$ | 2456677.727712 ±0.00022 | Transit midpoint ($\mathrm{BJD_{TDB}}$) | Dragomir et al. (2015) |
| $T_{14}$ | 0.07992 ±0.001 | Transit duration (days) | Dragomir et al. (2015) |
| $P$ | 3.3366413 ±0.0000060 | Period (days) | Dragomir et al. (2015) |
| $e$ | 0.114 ±0.052 | Eccentricity | Kosiarek et al. (2019) |
| $\omega$ | $-1.44^{+0.1}_{-0.04}$ | Argument of periastron (radians) | Kosiarek et al. (2019) |
| $K$ | $8.21^{+0.47}_{-0.46}$ | RV semi amplitude ( $\mathrm{m\,s^{-1}}$) | Kosiarek et al. (2019) |
| $M_{pl}$ | $12.58^{+1.31}_{-1.28}$ | Mass of the planet ($M_\oplus$) | Kosiarek et al. (2019) |
| $b$ | $0.47^{+0.074}_{-0.110}$ | Impact Parameter | Dragomir et al. (2015) |

one of the out-of-transit epochs is also shown in Figure 1. These data are processed the same way as other in-transit spectra, and we do not see any signatures of absorption inside the He 10830 Å triplet window.

### 3.2. *Column Density Measurement from Equivalent Width Analysis*

We measure the integrated equivalent width (EW) of the detected broad absorption in the vacuum wavelength range (10831.9 Å to 10833.6 Å ) in Figure 1 to be 0.012 ±0.002Å . We ignored the J=0 line (10832.06 Å in vacuum) of the triplet since its oscillator strength is only $1/8^{th}$ of the other two lines combined, so it is below our continuum noise (J=0 line is the dashed orange line in Figure 1). The resonant scattering absorption of He I 10830 Å is directly proportional to the number density of He I in the $^2_3S$ metastable triplet state. We use the curve of growth analysis in the optically thin regime to estimate the column density of He $^2_3S$ metastable atoms,

$$N_{He^2_3S} = \frac{\mathrm{EW}}{8.85 * 10^{-13}} \frac{1}{\lambda_2^2 \times f_{ik_2} + \lambda_3^2 \times f_{ik_3}}\ \mathrm{cm}^{-2}, \quad (1)$$

where $N_{He^2_3S}$ is the column density of He $^2_3S$ metastable atoms in $\mathrm{cm}^{-2}$, EW is the measured combined equivalent width of J=1 and J=2 lines of He 10830 Å triplet in units of Å, $\lambda_2$ and $\lambda_3$ are the wavelengths of the J=1 and J=2 triplet lines in units of microns, and $f_{ik_2}$ and $f_{ik_3}$ are the oscillator strengths of the lines taken from the NIST Atomic Spectra Database Lines Database (Drake 2006).

Substituting our measured EW, we obtain $N_{He^2_3S} = 2.4 \times 10^{10}\ \mathrm{cm}^{-2}$. This measured EW is a flux weighted average across the unresolved stellar disc during the transit. Hence, the column density we measure is also a stellar disc flux weighted average column density of the exosphere during the transit.

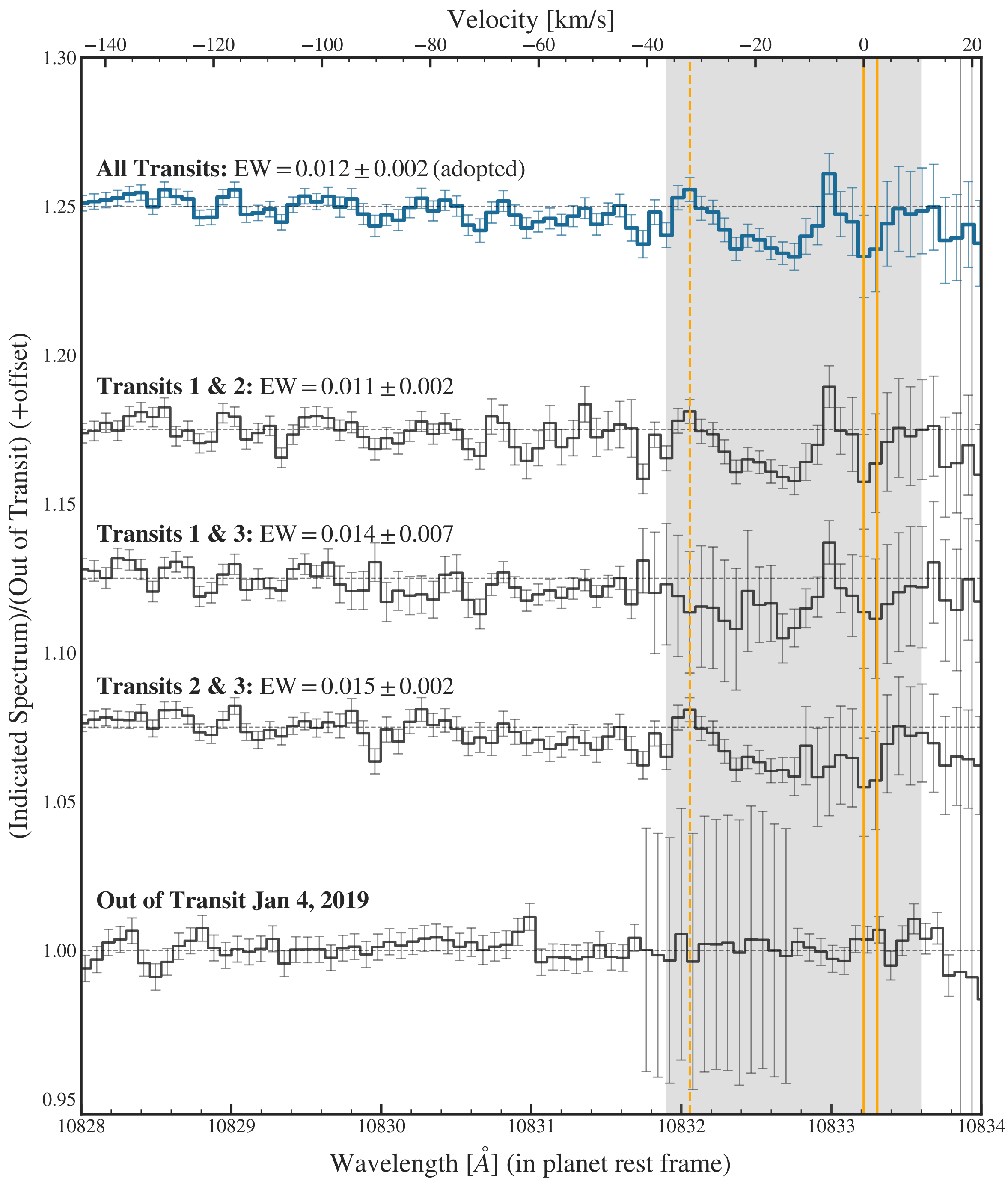


**Figure 1.** Detection of broad He 10830 absorption (EW: 0.012 ±0.002Å) in the wavelength range 10832.2 to 10833.4 Å in the in-transit / out-transit spectrum during three transits of GJ 3470b. The x-axis shows vacuum wavelength in planet's rest frame at mid-transit. The rest vacuum wavelengths of the He 10830 Å triplet lines in planet's rest frame are marked by the vertical dash and solid orange lines. The grey region highlights the detected absorption, and it is the wavelength window we used to measure reported equivalent widths. An out-of-transit epoch divided by the reference out-of-transit spectrum is also shown at the bottom, demonstrating the lack of any absorption in out-of-transit data.

### 3.3. *Theoretical Column Density from an Exosphere Model*

We modeled the steady state Helium distribution in the outflowing exosphere of GJ 3470b using the formalism and state transition coefficients outlined in Oklopčić & Hirata (2018). Using hydrodynamic simulations, Salz et al. (2016) show that the exosphere of GJ 3470b is not isothermal. We therefore do not use a Parker wind model for our atmospheric analysis, but solve for the steady state Helium distribution using the velocity and density field of the exosphere from the Salz et al. (2016) `PLUTO-CLOUDY` hydrodynamic simulations. To be internally consistent, we also used the GJ 3470 stellar SED used by Salz et al. (2016).

The X-ray spectrum of GJ 3470 we used from Salz et al. (2016) is calculated using the plasma emission model from `CHIANTI` (Dere et al. 1997, 2009) normalised to the X-ray luminosity of GJ 3470b estimated based on the stellar rotation period and the stellar mass (Pizzolato et al. 2003). The EUV flux (100 Å to ∼912 Å), which is critical for these calculations due to the strong dependence of Helium ionization, comes from the scaling of the model-dependent Ly$\alpha$ flux (Linsky et al. 2014). The model-dependent Ly$\alpha$ flux of GJ 3470 itself is estimated by the Linsky et al. (2013) model based on the X-ray luminosity. See Section 2.2 of Salz et al. (2016) for more details. This model-dependent irradiance spectrum of GJ 3470 is the source of the biggest uncertainty in our calculations. However, the model-dependent Ly$\alpha$ flux Salz et al. (2016) derive, and the value we adopt here, is consistent with the Ly$\alpha$ flux measured by Bourrier et al. (2018) during three transits of GJ 3470b using the Space Telescope Imaging Spectrograph instrument on board the Hubble Space Telescope (HST).

As most of the free electrons in the atmospheres of exoplanets come from ionized Hydrogen, to obtain the electron density of GJ 3470 atmosphere, we first solved for the steady-state of Hydrogen following Oklopčić & Hirata (2018). To obtain the steady state distribution of Helium atoms, we briefly discuss here the relevant system of integro-differential equations from Oklopčić & Hirata (2018), given by,

$$v\frac{\partial f_1}{\partial r} = (1 - f_1 - f_3)n_e\alpha_1 + f_3A_{31} - f_1\Phi_1e^{-\tau_1} - f_1n_eq_{13a} + f_3n_eq_{31a} + f_3n_eq_{31b} + f_3n_{H^0}Q_{31}, \tag{2}$$

and,

$$v\frac{\partial f_3}{\partial r} = (1 - f_1 - f_3)n_e\alpha_3 - f_3A_{31} - f_3\Phi_3e^{-\tau_3} + f_1n_eq_{13a} - f_3n_eq_{31a} - f_3n_eq_{31b} - f_3n_{H^o}Q_{31}, \tag{3}$$

where $f_1$ and $f_3$ are the fractions of neutral Helium in the ground state of the singlet and triplet states, respectively, $v$ is the velocity of the out-flowing exosphere as a function of radius we adopt from Salz et al. (2016), $n_e$ is the density of free electrons we obtained by solving the steady-state of Hydrogen, and $\alpha_1$ and $\alpha_3$ are the Helium recombination rates to singlet and triplet state from Osterbrock & Ferland (2006), respectively. The collision coefficients $q_{ijk}$ and $Q_{31}$ are from Oklopčić & Hirata (2018), calculated using coefficients from Bray, I. et al. (2000); Roberge & Dalgarno (1982). The radiative decay rate $A_{31}$ from the Helium metastable state to singlet state is adopted from Drake (1971). $\Phi_1$ and $\Phi_3$ are the effective photoionization rate coefficients calculated using,

$$\Phi_i = \int_{\lambda_1}^{\lambda_2} \frac{\lambda F_\lambda}{hc} a_\lambda d\lambda, \tag{4}$$

where, $F_\lambda$ is the irradiated flux on GJ3470b described earlier in this section, $a_\lambda$ is the photoionisation cross section taken from Brown (1971) for the singlet state, and from Norcross (1971) for the triplet state. For the singlet state, the integral is evaluated up to the ionisation wavelength of Helium (504 Å), while for the triplet state the integral is computed in the interval starting at Lyman limit[1] (911.6 Å) to the metastable state ionization wavelength (2583 Å).

To calculate the optical depths $\tau_1$ and $\tau_3$ as a function of radius for the singlet and metastable states of Helium, we compute the following integrals,

$$\begin{aligned}\tau_1 = a_{oH}\frac{0.9}{1.297 * m_p}\int_r^\infty (1 - f_{H+})\rho(r)dr \\ + a_{oHe}\frac{0.1}{1.297 * m_p}\int_r^\infty f_1\rho(r)dr,\end{aligned} \tag{5}$$

and,

$$\tau_3 = a_{oHe2S3}\frac{0.1}{1.297 * m_p}\int_r^\infty f_3\rho(r)dr, \tag{6}$$

where $m_p$ is the proton mass, $\rho(r)$ is the density of the GJ3470b exosphere from Salz et al. (2016), $f_{H+}$ is the fraction of ionized Hydrogen we obtained by solving the steady-state of Hydrogen. $a_{oH}$ and $a_{oHe}$ are GJ3470b's irradiation flux-averaged Hydrogen and Helium ionisation cross sections in the wavelength range up to Helium ionisation (504 Å). $a_{oHe2S3}$ is the flux-averaged cross section of He $^2_3S$ in the wavelength range 911.6 Å (hydrogen ionisation) to 2583 Å (He $^2_3S$ ionisation).

We solve Equations 2 & 3 iteratively as an initial boundary value partial differential equation by starting with an initial estimate for the optical depth integral term (Equations 5 & 6). Using the resulting solution, we updated the integral term in Equations 5 & 6. The final solutions converged within one or two iterations since the integral term has impact only in the high opacity base region of the outflowing atmosphere. The differential equation of He $^2_3S$ metastable atoms (Equation 3) is very stiff for high densities of GJ 3470b, and we therefore we used a Radau solver with adaptive dense gridding (Hairer & Wanner 1996).

The one dimensional radial density distribution of He $^2_3S$ metastable atoms obtained above is then integrated assuming a spherical exosphere to obtain column densities at different impact parameters from the planet (Figure 2b). We expect the model to fail beyond the Roche-lobe due to complex stellar wind interactions. We estimate the volume-equivalent Roche-lobe radius of the GJ 3470b system to be 3.12 $R_p$ following Eggleton (1983). The teardrop shaped Roche-lobe's extent on the star-planet axis is 5.96 $R_p$ (Salz et al. 2016). Both of these points are explicitly highlighted in Figure 2. Assuming an impact parameter of $b = 0.47$ (Dragomir et al. 2015), Figure 2a shows the 2D projection of the system during the midpoint of the transit. In Figure 2a we also illustrate the stellar disc on top of the column density map of He $^2_3S$ metastable atoms. To estimate the flux-averaged column density, we used a quadratic limb darkening model where we calculated the limb-darkening coefficients using the EXOFAST web-applet[2] using the stellar effective temperature, metallicity and surface gravity from Table 1, in the $J$ band. This flux-weighted average column density is dependent on how far the exosphere extends beyond the Roche-lobe; the predicted background stellar disc flux-weighted average column density of He $^2_3S$ metastable atoms as a function of the extent of GJ 3470b's exosphere is shown by the dashed line in Figure 2b).

#### 3.3.1. *Limits of the Model*

[1] Photons of energy higher than Lyman limit are many orders of magnitude more likely to be absorbed by the Hydrogen than He$^2_3$S, hence the beginning of the integral window was chosen to be at 911.6 Å

[2] http://astroutils.astronomy.ohio-state.edu/exofast/limbdark.shtml

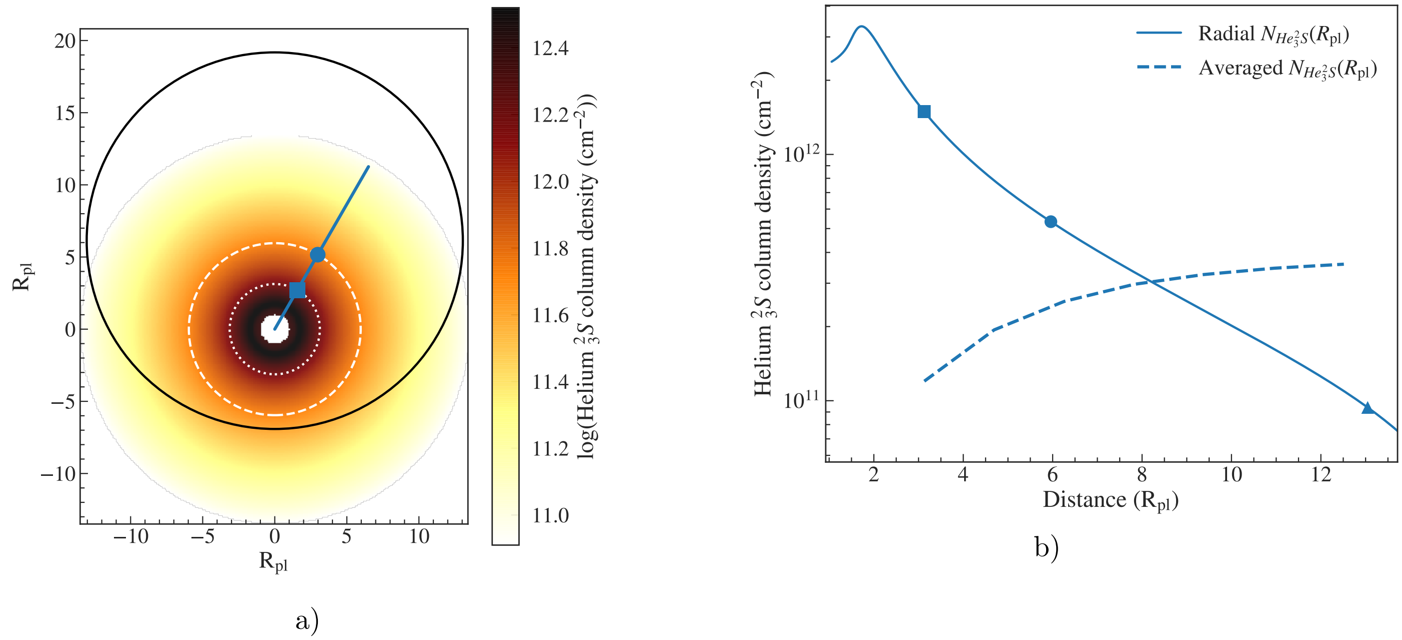


**Figure 2.** a) The 2D diagram showing the projection of the Roche lobe radii as well as the GJ3470 stellar disc on top of the spherical 1D He $^2_3S$ metastable atom column density map predicted by our 1D simulation of GJ 3470b. The volume equivalent Roche lobe radius as well as the Roche lobe extent on the star-planet axis is marked by the dot and dashed circles respectively. The large circle marks the disc of the star. b) The radial cut plot of the column density along the blue line in left figure is shown here as "Radial $N_{He^2_3S}$". The volume equivalent Roche lobe radius as well as the Roche lobe extend on the star-planet axis is marked by the square and dot respectively. The triangle marks the radius of the star. The dashed line shows the background stellar disc flux averaged column density predicted by our model at the center of the transit. It is a function of the assumed extent of the exo-sphere beyond the volume-equivalent Roche lobe as shown on left.

The simplified one dimensional model we presented here is to check whether the strength of our detected Helium 10830 Å absorption in the exo-planet atmosphere is within the limits of expected physical conditions. A true three dimensional wind model where the stellar irradence is only on one side of planet is known to have lesser density on an average in all angles by a factor of 4 than the one dimensional symmetric wind model we used (Stone & Proga 2009).

The other major source of uncertainty in our model is the irradiated flux in the wavelengths shorter than Helium ionization ($\lambda < 512$ Å). As briefly outlined in the section above, it is estimated by a chain of empirical models. We expect the Helium ionization flux to have a significant influence on the population of metastable He atoms. To study the impact, we simulated how the predicted column density of He $^2_3S$ metastable atoms changes when we suppress the irradience at wavelength shorter than 504 Å by different factors[3]. Results are shown in Figure 3. Since we wanted to probe only the impact on

[3] The reason we chose 504 Å for this test instead of 512 Å is because photons of energy higher than 504 Å are more likely to ionize a Helium atom than Hydrogen atom due to the factor of 10 lower abundance of Helium than Hydrogen. We want to probe the impact on Helium ionization alone without significant change to Hydrogen ionization.

the steady state of Helium atoms, the underlying velocity field and density used in the differential equation was kept fixed, and is the same as the Salz et al. (2016) hydrodynamic model for the original irradiance. It is very instructive to see that the observed column density of metastable Helium is reduced proportionally to the reduction in the Helium ionization flux.

In real systems, since the mass outflow is proportional to the energy absorbed in the lower atmosphere from irradiance, there will be an additional proportional reduction in density when the EUV flux irradiation is reduced. Hence, the combined effect of reduction in Helium ionizing radiation is quadratic on the column density of meta-stable Helium atoms.

A few more ways the underlying density of the wind we used in our simulation from Salz et al. (2016) can be impacted is summarized in Table 2 of Salz et al. (2016).

### 3.4. *Velocity of the Outflow*

The helium absorption we see in GJ 3470b is the broadest He 10830 Å absorption reported in the literature to date. It spans a velocity range of -36 km/sec to +9 km/sec. Figure 4a shows the outflowing exosphere velocity from Salz et al. (2016). The wind reaches only velocities up to ∼10 km/s inside 3.12 $R_p$—the volume-equivalent Roche-lobe radius. Both the volume equivalent Roche lobe radius as well as the Roche lobe extent on the star-planet axis (5.96 $R_p$) is marked by vertical lines in the plot.

The line of sight velocity of the Helium atoms we see during the transit is the sum of the hydrodynamic driven wind velocity plus the stellar radiative acceleration, and the planet's orbital radial velocity at the instant of their escape from the planet's gravitational potential. Helium atoms escaping the planet potential ∼2.5 hours before the transit will have a line of sight velocity of ∼-30 km/s during the transit due to change in the line of sight component of planet's orbital velocity. Figure 4b shows the time a Helium atom will take to travel the distance based on the wind model after it leaves the Roche lobe. Atoms which escape the potential 2.5 hours before the transit will be at ∼8 $R_p$, which is well within the projected stellar disc. Hence the observed blue shifted velocity is consistent with our model.

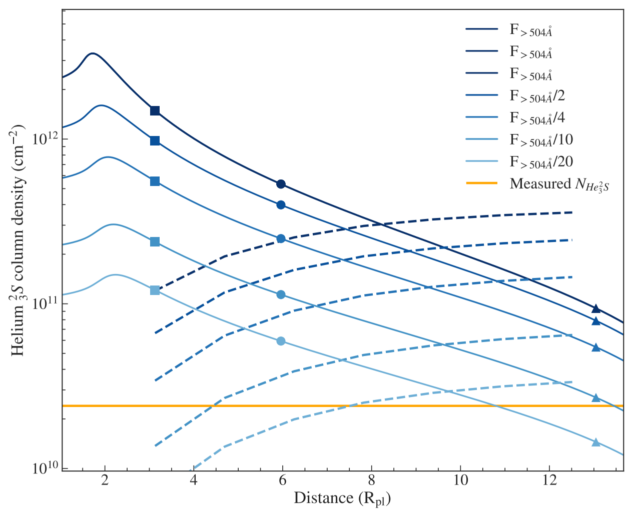


**Figure 3.** The column density of He $^2_3S$ metastable atoms predicted by the 1D simulation of GJ 3470b is reduced proportionally to the flux in wavelengths less than 504 Å when everything else—including the density and velocity—is kept fixed. The volume equivalent Roche lobe radius as well as the Roche lobe extent on the star-planet axis is marked by the square and dot respectively. The triangle marks the radius of the star. The dashed lines show the flux averaged column density predicted by this model at the center of the transit as a function of the extent of the exo-sphere beyond volume-equivalent Roche lobe. The horizontal orange line shows the measured average column density in transits of GJ 3470b using HPF.

### 3.5. *On the Difference Between the Predicted and Measured Column Densities*

As described in Section 3.2, the measured flux weighted column density of He $^2_3$S is $N_{He^2_3S} = 2.4 \times 10^{10} \mathrm{cm}^{-2}$. This is a factor of 10 less than predicted by our one dimensional hydrodynamic model described in Section 3.3. However, as dis-

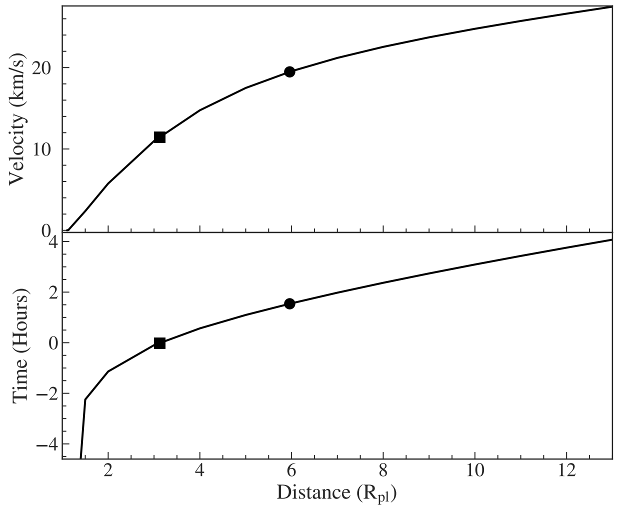


**Figure 4.** The top panel shows the one dimensional wind velocity model for GJ 3470b from Salz et al. (2016). The volume equivalent Roche lobe radius as well as the Roche lobe extent on the star-planet axis is marked by the square and dot respectively. The lower panel shows the time of flight for a Helium atom to reach a certain radius from the volume equivalent Roche lobe radius.

cussed in Section 3.3.1, if we correct our simulation for the 3D model simplification to 1D model by the factor of 4 (Stone & Proga 2009), and assume the Helium ionisation radiation is lesser by a factor of 1.6 (which is well within the error of the empirically derived EUV SED of GJ3470 in Salz et al. (2016)), we reduce the predicted metastable Helium by a factor of $4 \times 1.6^2 = 10$. Hence, our observations are consistent with our simplified model under the caveats outlined in Section 3.3.1.

## 4. CONCLUSION

We report the detection of He 10830 Å absorption from meta-stable Helium atoms in the base of the outflowing exosphere of the M dwarf planet GJ 3470b in three transits using the Habitable-zone Planet Finder (HPF) near-infrared spectrograph at the 10m Hobby-Eberly Telescope at McDonald Observatory. This measurement marks the first detection of He 10830 absorption in an M-dwarf planet. Further, we detect the Helium absorption in the velocity range of -36 km/sec to +9 km/sec, marking the largest blueshift of He 10830 absorption reported so far in the literature. From our observed absorption, we measure an equivalent width of EW $= 0.012 \pm 0.002 \AA$, corresponding to a disc surface flux-averaged column density of $N_{He^2_3S} = 2.4 \times 10^{10}\,\mathrm{cm}^{-2}$. Both the velocity range and the column density we measure are consistent with our exosphere model based on the work of Salz et al. (2016) and Oklopčić & Hirata (2018) to within the model uncertainties of the UV and X-ray flux of GJ 3470.

The authors wish to thank M. Salz and A. Oklopčić for discussions that contributed to this work.

This work was partially supported by funding from the Center for Exoplanets and Habitable Worlds. The Center for Exoplanets and Habitable Worlds is supported by the Pennsylvania State University, the Eberly College of Science, and the Pennsylvania Space Grant Consortium. We acknowledge support from NSF grants AST-1006676, AST-1126413, AST-1310885, AST-1517592, AST-1310875, the NASA Astrobiology Institute (NAI; NNA09DA76A), PSARC, and NIST in our pursuit of precision radial velocities in the NIR. Computations for this research were performed on the Pennsylvania State Universitys Institute for CyberScience Advanced CyberInfrastructure (ICS-ACI). We acknowledge support from the Heising-Simons Foundation via grant 2017-0494. This work was supported by NASA Headquarters under the NASA Earth and Space Science Fellowship Program through grants NNX16AO28H and 80NSSC18K1114.

These results are based on observations obtained with the Habitable-zone Planet Finder Spectrograph on the Hobby-Eberly Telescope. We thank the Resident astronomers and Telescope Operators at the HET for the skillful execution of our observations of our observations with HPF. The Hobby-Eberly Telescope is a joint project of the University of Texas at Austin, the Pennsylvania State University, Ludwig-Maximilians-Universitt Mnchen, and Georg-August Universitt Gottingen. The HET is named in honor of its principal benefactors, William P. Hobby and Robert E. Eberly. The HET collaboration acknowledges the support and resources from the Texas Advanced Computing Center.

This research has made use of NASA's Astrophysics Data System Bibliographic Services.

Software: barycorrpy (Kanodia & Wright 2018), astropy (Astropy Collaboration et al. 2018), numpy (van der Walt et al. 2011), scipy (Jones et al. 2001–), matplotlib (Hunter 2007), CoCalc (SageMath 2019).

*Facilities:* HET (HPF)

## REFERENCES


Allart, R., Bourrier, V., Lovis, C., et al. 2018, Science, 362, 1384

—. 2019, A&A, 623, A58

Astropy Collaboration, Price-Whelan, A. M., Sipőcz, B. M., et al. 2018, AJ, 156, 123

Awiphan, S., Kerins, E., Pichadee, S., et al. 2016, MNRAS, 463, 2574

Bender, C. F., Mahadevan, S., Deshpande, R., et al. 2012, ApJL, 751, L31

Biddle, L. I., Pearson, K. A., Crossfield, I. J. M., et al. 2014, MNRAS, 443, 1810

Bourrier, V., Lecavelier des Etangs, A., Ehrenreich, D., et al. 2018, A&A, 620, A147

Bray, I., Burgess, A., Fursa, D. V., & Tully, J. A. 2000, Astron. Astrophys. Suppl. Ser., 146, 481. https://doi.org/10.1051/aas:2000277

Brown, R. L. 1971, ApJ, 164, 387

Clough, S., Shephard, M., Mlawer, E., et al. 2005, Journal of Quantitative Spectroscopy and Radiative Transfer, 91, 233 . http://www.sciencedirect.com/science/article/pii/S0022407304002158

Dere, K. P., Landi, E., Mason, H. E., Monsignori Fossi, B. C., & Young, P. R. 1997, A&AS, 125, 149

Dere, K. P., Landi, E., Young, P. R., et al. 2009, A&A, 498, 915

Dragomir, D., Benneke, B., Pearson, K. A., et al. 2015, ApJ, 814, 102

Drake, G. 2006, High Precision Calculations for Helium, ed. G. Drake (New York, NY: Springer New York), 199–219. https://doi.org/10.1007/978-0-387-26308-3_11

Drake, G. W. F. 1971, Phys. Rev. A, 3, 908. https://link.aps.org/doi/10.1103/PhysRevA.3.908

Eggleton, P. P. 1983, ApJ, 268, 368

Ehrenreich, D., Bourrier, V., Wheatley, P. J., et al. 2015, Nature, 522, 459. https://www.nature.com/articles/nature14501

Gaia Collaboration, Brown, A. G. A., Vallenari, A., et al. 2018, A&A, 616, A1

Hairer, E., & Wanner, G. 1996, Solving Ordinary Differential Equations II. Stiff and Differential-Algebraic Problems, Vol. 14, doi:10.1007/978-3-662-09947-6

Hunter, J. D. 2007, Computing in Science and Engineering, 9, 90

Jones, E., Oliphant, T., Peterson, P., et al. 2001–, SciPy: Open source scientific tools for Python, , . http://www.scipy.org/

Kanodia, S., & Wright, J. 2018, Research Notes of the American Astronomical Society, 2, 4

Kaplan, K. F., Bender, C. F., Terrien, R., et al. 2018, in The 28th International Astronomical Data Analysis Software & Systems

Kosiarek, M. R., Crossfield, I. J. M., Hardegree-Ullman, K. K., et al. 2019, AJ, 157, 97

Kulow, J. R., France, K., Linsky, J., & Loyd, R. O. P. 2014, ApJ, 786, 132

Linsky, J. L., Fontenla, J., & France, K. 2014, ApJ, 780, 61

Linsky, J. L., France, K., & Ayres, T. 2013, ApJ, 766, 69

Mahadevan, S., Ramsey, L. W., Terrien, R., et al. 2014, in Proc. SPIE, Vol. 9147, Ground-based and Airborne Instrumentation for Astronomy V, 91471G

Mansfield, M., Bean, J. L., Oklopčić, A., et al. 2018, ApJL, 868, L34

Metcalf, A. J., Anderson, T., Bender, C. F., et al. 2019, arXiv e-prints, arXiv:1902.00500

Moutou, C., Coustenis, A., Schneider, J., Queloz, D., & Mayor, M. 2003, Astronomy & Astrophysics, 405, 341. https://www.aanda.org/articles/aa/abs/2003/25/aa3416/aa3416.html

Ninan, J. P., Bender, C. F., Mahadevan, S., et al. 2018, in Society of Photo-Optical Instrumentation Engineers (SPIE) Conference Series, Vol. 10709, High Energy, Optical, and Infrared Detectors for Astronomy VIII, 107092U

Norcross, D. W. 1971, Journal of Physics B: Atomic and Molecular Physics, 4, 652. https://doi.org/10.1088%2F0022-3700%2F4%2F5%2F006

Nortmann, L., Pallé, E., Salz, M., et al. 2018, Science, 362, 1388

Oklopčić, A., & Hirata, C. M. 2018, The Astrophysical Journal Letters, 855, L11. http://stacks.iop.org/2041-8205/855/i=1/a=L11

Osterbrock, D. E., & Ferland, G. J. 2006, Astrophysics Of Gas Nebulae and Active Galactic Nuclei (University science books)

Pizzolato, N., Maggio, A., Micela, G., Sciortino, S., & Ventura, P. 2003, A&A, 397, 147

Ramsey, L. W., Adams, M. T., Barnes, T. G., et al. 1998, in Proc. SPIE, Vol. 3352, Advanced Technology Optical/IR Telescopes VI, ed. L. M. Stepp, 34–42

Roberge, W., & Dalgarno, A. 1982, ApJ, 255, 489

SageMath, I. 2019, CoCalc Collaborative Computation Online, https://cocalc.com/

Salz, M., Czesla, S., Schneider, P. C., & Schmitt, J. H. M. M. 2016, A&A, 586, A75

Salz, M., Czesla, S., Schneider, P. C., et al. 2018, A&A, 620, A97

Seager, S., & Sasselov, D. D. 2000, The Astrophysical Journal, 537, 916. http://stacks.iop.org/0004-637X/537/i=2/a=916

Shetrone, M., Cornell, M. E., Fowler, J. R., et al. 2007, PASP, 119, 556

Spake, J. J., Sing, D. K., Evans, T. M., et al. 2018, Nature, 557, 68

Stone, J. M., & Proga, D. 2009, ApJ, 694, 205

van der Walt, S., Colbert, S. C., & Varoquaux, G. 2011, Computing in Science Engineering, 13, 22

Vidal-Madjar, A., des Etangs, A. L., Dsert, J.-M., et al. 2003, Nature, 422, 143. https://www.nature.com/articles/nature01448